Pergamon

Geothermics, Vol. 26, No. 4, pp. 437–464, 1997

Published by Elsevier Science Ltd

0375–6505/97 $17.00 + 0.00

PII: S0375–6505(97)00007–2

THE SIMULATOR TOUGH2/EWASG FOR MODELLING GEOTHERMAL RESERVOIRS WITH BRINES AND NON-CONDENSIBLE GAS

ALFREDO BATTISTELLI,* CLAUDIO CALORE† and KARSTEN PRUESS‡

* *Aquater S.p.A., 53 Via Miralbello, 61047 S. Lorenzo in Campo (PS), Italy;*
† *International Institute for Geothermal Research—CNR, 2 Piazza Solferino, 56126 Pisa, Italy; and* ‡ *Earth Sciences Division, Lawrence Berkeley National Laboratory, One Cyclotron Road, Berkeley, CA 94720, U.S.A.*

(*Received July* 1996; *accepted for publication January* 1997)

Abstract—An equation-of-state (EOS) module has been developed for the TOUGH2 simulator, belonging to the MULKOM family of computer codes developed at Lawrence Berkeley National Laboratory. This module, named EWASG (Equation-of-State for Water, Salt and Gas), is able to handle three-component mixtures of water, sodium chloride, and a slightly soluble non-condensible gas (NCG). At present the NCG can be chosen to be air, CO_2, CH_4, H_2, or N_2. EWASG can describe liquid and gas phases, and includes precipitation and dissolution of solid salt. The dependence of density, viscosity, enthalpy, and vapour pressure of brine on salt concentration is taken into account, as well as the effects of salinity on gas solubility in the liquid phase and related heat of solution. The reduction of rock porosity because of salt precipitation is also considered, as well as the related decrease of formation permeability. Vapour pressure lowering (VPL) due to suction pressure is represented by Kelvin's equation, in which the effects of salt are considered whereas those of NCG have currently been neglected.

The main assumptions made in developing the EWASG module are described, together with the correlations employed to calculate the thermophysical properties of multiphase H_2O–NaCl–CO_2 mixtures, which can be used to simulate the thermodynamic behaviour of commonly exploited geothermal reservoirs. © 1997 *CNR. Published by Elsevier Science Ltd.*

Key words: TOUGH2, numerical simulator, multicomponent fluid, reservoir simulation, modelling.

NOMENCLATURE

$A(i)$	coefficients in the polynomial fit of salt mass fraction at critical temperature
$B(i)$	coefficients in the polynomial fit of Henry's constant
$C(i)$	coefficients in the polynomial fit of salting-out coefficient
c	compressibility of liquid phase [Pa^{-1}]

C	specific heat [J/(kg °C)]
d_{nm}	distance between nodal points n and m [m]
$D_{\kappa\kappa'}$	diffusion coefficient [m^2/s]
$\mathbf{f}^{(\kappa)}$	binary diffusive flux of component κ [kg/(m^2 s)]
f_{VPL}	vapour pressure lowering factor
$\mathbf{F}^{(\kappa)}$	flux of component κ [kg/(s m^2) or J/(s m^2)]
$\mathbf{g}$	acceleration of gravity [m/s^2]
h	layer thickness [m]
H	specific enthalpy [J/kg]
k	intrinsic permeability [m^2]
k_{b}	salting-out coefficient [kg/mol]
K	thermal conductivity [W/(m °C)]
K_{h}	Henry's constant [Pa]
$k_{r\beta}$	relative permeability to phase β
m	salt molality [mol/kg]
$M^{(\kappa)}$	accumulation term of component κ [kg/m^3 or J/m^3]
$\mathbf{n}$	unit normal vector
NK	number of mass components
NPH	number of phases
P	pressure [Pa]
P_{cap}	capillary pressure [Pa]
P_{wb}	wellbore pressure [Pa]
PI	productivity index [m^3]
q	production rate [kg/s]
$Q^{(\kappa)}$	sink or source volumetric rate of component κ [kg/(s m^3) or J/(s m^3)]
r_{e}	effective wellblock radius [m]
r_{w}	well radius [m]
R	universal gas constant [J/(mol K)]
s	skin factor
S	saturation
t	time [s]
T	temperature [°C]
u	specific internal energy [J/kg]
V_n	volume of grid element n [m^3]
$X^{(\kappa)}$	mass fraction of component κ
$X_{\mathrm{sol}}{}^{(2)}$	mass fraction of NaCl in halite-saturated brine
$Y^{(\kappa)}$	mole fraction of component κ
$W^{(\kappa)}$	molecular weight of component κ [kg/mol]
ΔH_{sol}	heat of solution [J/kg]
Γ_n	surface area of grid element n [m^2]
μ	dynamic viscosity [Pa s]
ρ	density [kg/m^3]
ϕ	porosity
τ	tortuosity factor

Subscripts and superscripts

a	active
b	brine
boil	boiling
β	phase index (liquid, gas, solid)

c	critical
eq	equivalent salt mass fraction
G	gas phase
κ	component index
L	liquid phase
R	rock grains
S	solid salt phase
sat	vapour-saturated
1	water component, H_2O
2	salt component, NaCl
3	gas component, NCG

INTRODUCTION

The thermodynamic and transport properties of geothermal fluids are very important for determining the natural state of a geothermal system and its behaviour under exploitation. Such fluids usually consist of complex mixtures of water, non-condensible gases (NCG) and salts dissolved in the liquid phase. As water always represents the main mixture component, its thermophysical properties have been customarily used to model geothermal reservoirs. In some cases, however, the content of other components is such that they can alter the reservoir performance significantly. Thus, it is necessary to include in the numerical simulation of such systems the effects of salts and NCG on their thermodynamic behaviour. Furthermore, the inclusion of salts and gases introduces additional constraints on modelling results, making them more unique. The spatial variations and transients of the concentration of chemicals can provide important information about fluid flow patterns in the reservoir, the location of upflow zones, mixing with colder fluids, reinjected fluid pathways, and boiling/condensation processes in different reservoir zones.

NCG in geothermal systems are mainly represented by CO_2, CH_4, H_2S, N_2, and H_2. Their concentration in reservoir fluid ranges from a few hundred ppm (wt.) up to several tens of thousands ppm, with carbon dioxide generally exceeding 90% by volume of total NCG. For this reason CO_2 is generally chosen to describe the overall effects of NCG in geothermal reservoir simulation. The effects of CO_2 have been included in numerical reservoir simulators by several authors (Zyvoloski and O'Sullivan, 1980; Pritchett *et al.*, 1981; O'Sullivan *et al.*, 1985; Alkan *et al.*, 1995; Moya *et al.*, 1995).

The importance of salt content has received less attention in reservoir modelling, mainly because only a few high-salinity reservoirs have been exploited up to now. Dissolved solids content in reservoir brines ranges from a few thousand ppm (wt.) up to 280,000 ppm in the Salton Sea hypersaline geothermal reservoir. Apart from low-salinity systems, where carbonatic species and silica are often predominant in the liquid phase, the main dissolved solids are Na, K, and Ca chlorides, sodium chloride being the predominant salt. For this reason the thermodynamic properties of sodium chloride solutions are customarily used in the simulation of geothermal reservoirs to represent the effects of total dissolved solids.

Although the main effects of dissolved solids and NCG on fluid mixture properties are well known, the quantitative evaluation of the effect of variable proportions of both salinity and non-condensible gases on reservoir conditions and performance requires additional studies.

Capillary pressure and vapour adsorption effects, here referred to as suction pressure

effects, and associated vapour pressure lowering (VPL) phenomena are believed to be of major importance in determining the in-place and extractable fluid reserves of vapour-dominated reservoirs (Satik *et al.*, 1996). Modelling studies of the effects of capillarity and vapour adsorption on the depletion of vapour-dominated geothermal reservoirs have been performed by Pruess and O'Sullivan (1992), considering pure water.

For the compositional simulation approach required to study saline natural systems that also contain an NCG, an equation-of-state (EOS) module, named EWASG, was developed in 1992 for LBNL's multipurpose TOUGH2 numerical reservoir simulator by Battistelli *et al.* (1993) and enhanced in 1994 by including VPL due to suction pressure (Battistelli *et al.*, 1995). The module has been developed using NaCl to simulate the effects of dissolved salts. The effect of NCG has been included following a general formulation in which a different NCG can, in principle, be simulated by implementing the equations describing its specific thermophysical properties in the existing subroutines. At present the NCG can be chosen from air, CO_2, CH_4, H_2, or N_2. Possible applications of the EWASG module include the simulation of saline systems containing an NCG, such as conventional high-temperature geothermal reservoirs (CO_2), low-temperature geothermal reservoirs (CO_2 or CH_4), an unsaturated zone (air), and nuclear waste repositories (air or H_2). Another gaseous species that is relevant to geochemical studies of geothermal systems is H_2S. This has not been included in the present version of the EWASG module because: (a) this module can handle one NCG component only, and generally the most abundant gas species in geothermal systems is CO_2; and (b) the formulation adopted in EWASG does not account for chemical reactions, which, for a reactive species such as H_2S, are very important.

Other codes are available to simulate the behaviour of multi-component systems. Andersen *et al.* (1992) presented a PVT model for H_2O–NaCl–CO_2 mixtures. The possible precipitation of solid salt was not accounted for. Their EOS module has been included in the TETRAD simulator and used by Shook (1995) to study the effects of salt on the formation of a high-temperature reservoir in vapour-dominated systems. An EOS module for H_2O–NaCl–CO_2 mixtures implementing salt precipitation and associated permeability changes is available for the STAR reservoir simulator (Pritchett, 1993). Studies are under way to set up a water–sodium chloride EOS module for the TOUGH2 simulator for high temperatures and pressures: McKibbin and McNabb (1993) presented an accurate description of phase boundaries of an H_2O–NaCl system up to 1075°C and 160 MPa. They recently extended their thermodynamic formulation by adding the carbon dioxide component (McKibbin and McNabb, 1995). A simulation capability for reactive chemical transport of dissolved solids and non-condensible gases was developed by White, and implemented in an enhanced version of the TOUGH2 code (White, 1994, 1995). Kissling *et al.* (1996) applied this capability to modelling of the Wairakei geothermal field.

This paper describes the main assumptions made in developing the EWASG module, together with the correlations employed to calculate the thermophysical properties of multiphase mixtures of water, sodium chloride and carbon dioxide. These correlations have been partially revised, with respect to previous module versions (Battistelli *et al.*, 1993, 1995), in order to extend their range of application over the P–T–X space of interest for the numerical simulation of geothermal reservoirs. The range of applicability of the present thermophysical formulation is: temperatures from 100 to 350°C, total pressure up to 80 MPa, partial pressure of CO_2 up to 10 MPa, and salt mass fraction up to halite saturation. The lower temperature limit (100°C) is a result of the correlation used for brine enthalpy, otherwise it could be less than 10°C. The methods used to model the reduction of

rock porosity due to salt precipitation and the related decrease of formation permeability, and vapour pressure lowering due to suction pressure in the presence of saline brines, are also illustrated. Numerical results of fluid production from geothermal reservoir blocks and related depletion behaviour will be presented in a later paper (Calore *et al.*, in preparation).

MODELLING APPROACH

The TOUGH2 code implements the general MULKOM architecture for coupled multiphase, multicomponent fluid and heat flows (Pruess, 1983, 1991a). Several EOS modules have been developed for treating different mixtures in order to solve problems in the fields of hydrogeology, geothermal and petroleum engineering, nuclear waste disposal, and environmental pollution (Pruess, 1995). The EWASG EOS module was developed to simulate flow problems in which the transport of a variable salinity brine and a slightly soluble NCG occurs. The multiphase system is assumed to be composed of three mass components: water, sodium chloride, and carbon dioxide, or some other NCG. Whereas water and the NCG components may be present only in the liquid and gas phases, the salt component may be dissolved in the liquid phase or precipitated to form a solid salt phase. The adsorption of water or NCG in the solid salt phase is neglected, as well as the small solubility of NaCl in the gas phase.

The three mass component formulation employed was developed by enhancing an already existing EOS module for simulating the non-isothermal flow of saline water and air (Pruess, 1991b). The treatment of precipitation/dissolution of sodium chloride has been introduced using the method employed to treat similar phenomena occurring for water–silica mixtures (Verma and Pruess, 1988). The reduction of rock porosity because of salt precipitation is taken into account, as well as the related decrease of formation permeability. The formulation of H_2O–CO_2 fluid mixture basically follows that described by O'Sullivan *et al.* (1985). The dependence of brine thermophysical properties on salt concentration has been included, following an updated version of the thermophysical package developed by Aquater for a wellbore numerical simulator (Battistelli, 1991). All relevant thermophysical properties are evaluated using a subroutine-by-subroutine structure, so that the correlations employed at present can be easily modified, as soon as more reliable experimental data and correlations become available. The dependence of brine enthalpy, density, viscosity and vapour pressure on salt concentration has been accounted for, as well as the effect on NCG solubility and heat of solution in the brine.

Transport of the mass components occurs by advection in liquid and gas phases; binary diffusion in the gas phase for steam and the NCG is accounted for. Diffusion in the liquid phase and hydrodynamic dispersion are not included in the publicly available version of TOUGH2. It is assumed that the three phases (gas, liquid, and solid) are in local chemical and thermal equilibrium, and that no chemical reactions take place other than interphase mass transfer.

In the integral finite differences formulation used by TOUGH2, the balance equations, for a system of NK mass components distributed in NPH phases, are written in the following general form (Pruess, 1991a):

$$\frac{\mathrm{d}}{\mathrm{d}t}\int_{V_n} M^{(\kappa)}\,\mathrm{d}V = \int_{\Gamma_n} \mathbf{F}^{(\kappa)}\cdot\mathbf{n}\,\mathrm{d}\Gamma + \int_{V_n} Q^{(\kappa)}\,\mathrm{d}V \tag{1}$$

The general form of the mass accumulation terms ($\kappa = 1, NK$) is as follows:

$$M^{(\kappa)} = \phi \sum_{\beta=1}^{NPH} S_\beta \rho_\beta X_\beta^{(\kappa)} \tag{2}$$

where $\beta = 1$, NPH is the phase index. The heat accumulation term ($\kappa = NK + 1$) in a multiphase system is

$$M^{(NK+1)} = \phi \sum_{\beta=1}^{NPH} S_\beta \rho_\beta u_\beta + (1 - \phi)\rho_R C_R T \tag{3}$$

The mass flux term is a sum over phases

$$\mathbf{F}^{(\kappa)} = \sum_{\beta=1}^{NPH} X_\beta^{(\kappa)} \mathbf{F}_\beta \tag{4}$$

Individual phase fluxes are given by a multi-phase version of Darcy's law

$$\mathbf{F}_\beta = -k \frac{k_{r\beta}}{\mu_\beta} \rho_\beta (\nabla P_\beta - \rho_\beta \mathbf{g}) \tag{5}$$

In addition to Darcy flow, TOUGH2 includes binary diffusion in the gas phase for fluids with two gaseous (or volatile) components κ, κ'

$$\mathbf{f}_{\beta=\text{gas}}^{(\kappa)} = -\phi S_G \tau D_{\kappa\kappa'} \rho_G \nabla X_G^{(\kappa)} \tag{6}$$

The heat flux contains conductive and convective components

$$\mathbf{F}^{(NK+1)} = \sum_{\beta=1}^{NPH} H_\beta \mathbf{F}_\beta + K \nabla T \tag{7}$$

In the EWASG module formulation $NK = 3$, $NPH = 3$, $\kappa = 1,2,3,4$ indicate water, NaCl, NCG and heat components, respectively, and $\beta = 1,2,3$ indicates the gas (G), liquid (L) and solid salt (S) phases, respectively. In particular, considering that the solubility of NaCl in the gas phase has been neglected and that the solid salt phase is not mobile, the accumulation and mass flux terms for the NaCl component ($\kappa = 2$) are written as follows:

$$M^{(2)} = \phi S_S \rho_S + \phi S_L \rho_L X_L^{(2)} \tag{8}$$

$$\mathbf{F}^{(2)} = -k \frac{k_{rL}}{\mu_L} \rho_L X_L^{(2)} (\nabla P_L - \rho_L \mathbf{g}) \tag{9}$$

where S_S is the "solid saturation", defined as the fraction of pore volume occupied by solid salt.

THERMODYNAMIC PACKAGE DESCRIPTION

For a system of three mass components distributed according to local thermodynamic equilibrium among three phases, four independent thermodynamic parameters, or primary variables, are necessary to identify the thermodynamic state. In a system of three coexisting phases, seven combinations are possible: three single-phase conditions, three liquid + gas conditions, and the three-phase condition. With the exclusion of the single-solid salt phase, which is not of interest for exploitation of geothermal reservoirs, the EWASG module is able to handle the six remaining phase combinations.

Table 1. Primary variable sets in EWASG (Equation-of-State module for Water, Salt and Gas)

Thermodynamic conditions	Primary variables			
	1	2	3	4
Liquid	P_L	$X_L^{(2)}$	$X_L^{(3)}$	T
Gas	P_G	$X_G^{(2)}$	$X_G^{(3)}$	T
Liquid + gas	P_G	$X_L^{(2)}$	S_G	T
Liquid + solid	P_L	S_S	$X_L^{(3)}$	T
Gas + solid	P_G	S_S	$X_G^{(3)}$	T
Liquid + gas + solid	P_G	S_S	S_G	T

The primary variables used in EWASG for single-phase conditions are total pressure, P, salt mass fraction, $X^{(2)}$, NCG mass fraction, $X^{(3)}$, and temperature, T. In liquid + gas conditions the third primary variable is switched from NCG mass fraction to gas phase saturation S_G. If the solid salt is present, the second primary variable is switched to solid saturation S_S. Table 1 summarises the sets of primary variables used by EWASG for each of the considered phase combinations. One point should be made with regard to the single-gas state: the salt mass fraction in the gas phase is used as second primary variable. As the NaCl solubility has been neglected in the gas phase, then $X_G^{(2)}$ must be equal to 0. If $X_G^{(2)} > 0$ then the solid salt phase appears and the primary variable is switched to solid saturation.

Mass balances of water, salt and NCG components, together with the heat balance, are set up and solved by TOUGH2 using the Newton–Raphson iteration method. During the iteration process, the EOS module must be capable of recognizing the appearance and disappearance of phases, and of providing all thermophysical properties of phases present, which are needed to assemble the balance equations, pertaining to the last updated primary variables. A description follows of the main tests performed to recognize the phase transitions and of the equations used to calculate phase properties.

With regard to the convention used for the thermodynamic state and the conditions to which enthalpies of single components are referred, we have considered the triple point of water, so that the enthalpies of liquid water, gaseous NCG and solid salt are zero at the following thermodynamic conditions: 0.01°C and 6 kPa.

Liquid conditions

Firstly, the test for possible phase change to two-phase conditions is made by checking whether the boiling pressure of the fluid mixture exceeds the total pressure. If

$$P < P_{\text{boil}}(T, X_L^{(2)}, X_L^{(3)}) \tag{10}$$

then the gas phase appears and the third primary variable is switched from NCG mass fraction $X_L^{(3)}$ to gas-phase saturation S_G, which is initialized to a small non-zero quantity. Actually, $10 + S_G$ is used as third primary variable; since it is larger than 1 it can be distinguished from NCG mass fraction, which is always lower than 1. The liquid-phase boiling pressure in equation (10) is given by

$$P_{\text{boil}} = P_{\text{b sat}}(T, X_L^{(2)}) + P^{(3)}(T, X_L^{(2)}, X_L^{(3)}) \tag{11}$$

where $P_{b\ sat}$ is the saturation pressure of brine and the bubbling pressure of NCG, $P^{(3)}$, is calculated according to Henry's law. The salting-out effect on Henry's law constant, i.e. the reduction of NCG solubility due to the presence of salt, is also accounted for.

The solid salt phase appears if the salt mass fraction in the liquid phase exceeds the halite solubility. If

$$X_L^{(2)} > X_{sol}^{(2)}(T) \tag{12}$$

precipitation starts and the second primary variable is switched from salt mass fraction $X_L{}^{(2)}$ to solid saturation S_S, which is initialized to a small non-zero value. In this case $10 + S_S$ is used as second primary variable in order to distinguish it from sodium chloride mass fraction. When solid phase is present, its disappearance is recognized simply by $S_S < 0$. In this case the second primary variable is switched back to $X_L{}^{(2)}$, and is initialized with a value slightly smaller than the NaCl solubility $X_{sol}{}^{(2)}(T)$.

The thermophysical properties of the liquid phase are calculated as follows. The density and viscosity are assumed to be the same as those for brine, with the assumption that the effect of dissolved gas can be neglected because of low gas solubility. Liquid phase density, viscosity and enthalpy are given by

$$\rho_L = \rho_b(P, T, X_L^{(2)}) \tag{13}$$

$$\mu_L = \mu_b(P, T, X_L^{(2)}) \tag{14}$$

$$H_L = (1 - X_L^{(3)})H_b(P, T, X_L^{(2)}) + X_L^{(3)}H_L^{(3)}(P^{(3)}, T) \tag{15}$$

Gas conditions

In single-phase gas conditions the salt component can be present only as solid precipitate, having neglected its solubility in the gas phase, which is very small in the temperature range of EWASG formulation. In fact, at 350°C the mass fraction of NaCl in the gas phase of a two-phase gas–liquid system reaches its maximum value at 15.5 MPa, amounting to 3.3×10^{-5}, whereas the mass fraction of NaCl in the brine is 9.41×10^{-2} and their ratio is 3.5×10^{-4} (Bischoff and Pitzer, 1989).

The possible appearance of the liquid phase is tested by checking the partial pressure of steam, $P^{(1)}$, against the vapour brine pressure. If

$$P^{(1)} > P_{b\ sat}(T, X_{eq}^{(2)}) \tag{16}$$

then the liquid phase appears and the third primary variable is switched from NCG mass fraction in the gas phase $X_G{}^{(3)}$ to gas-phase saturation, which is initialized to a value slightly smaller than $1 - S_S$.

The brine vapour pressure is calculated assuming $X_{eq}{}^{(2)} = 0$ if no solid phase is present in the element, otherwise the solubility of NaCl at element temperature is used. Partial pressure of the water component is calculated using an iterative procedure from total pressure, temperature and NCG mass fraction.

Density, viscosity and enthalpy of single-phase gas mixtures are calculated as follows:

$$\rho_G = \rho_G^{(1)}(P^{(1)}, T) + \rho_G^{(3)}(P^{(3)}, T) \tag{17}$$

$$\mu_G = (1 - X_G^{(3)})\mu_G^{(1)}(P^{(1)}, T) + X_G^{(3)}\mu_G^{(3)}(P^{(3)}, T) \tag{18}$$

$$H_G = (1 - X_G^{(3)})H_G^{(1)}(P^{(1)}, T) + X_G^{(3)}H_G^{(3)}(P^{(3)}, T) \tag{19}$$

Liquid–gas mixtures

For elements with two-phase fluid the phase transition test is made by checking the gas-phase saturation that is used as third primary variable. If $S_G \geq (1 - S_S)$, then the liquid phase disappears and a transition to single-phase gas conditions is made. If $S_G \leq 0$, then the gas phase disappears and a transition to single-phase liquid conditions is made. Appearance or disappearance of a precipitated solid phase is handled as in liquid conditions.

With the assumption of additivity of partial pressures, the partial pressure of NCG is given by

$$P^{(3)} = P - P_{b\,sat}(T, X_L^{(2)}) \tag{20}$$

The mole fraction of NCG in the liquid phase is calculated according to Henry's law

$$Y_L^{(3)} = P^{(3)}/K_{hb}(T, X_L^{(2)}) \tag{21}$$

Then the mass fraction of NCG in the liquid phase is calculated in an obvious way. The mass fraction of NCG in the gas phase is calculated from the density of fluid mixture, computed considering an ideal mixture of steam and gas

$$\rho_G = \rho_G^{(1)}(P_{b\,sat}, T) + \rho_G^{(3)}(P^{(3)}, T) \tag{22}$$

so that

$$X_G^{(3)} = \rho_G^{(3)}/\rho_G \tag{23}$$

The viscosity and specific enthalpy of the vapour phase are calculated using equations (18) and (19), respectively, with $P^{(1)} = P_{b\,sat}$.

The density, viscosity and enthalpy of the liquid phase are calculated with equations (13), (14) and (15), respectively, using the component mass fractions in the liquid phase.

THERMODYNAMIC PROPERTIES OF MIXTURE COMPONENTS

The correlations used to evaluate the thermophysical properties of phases in which the three components H_2O, NaCl and CO_2 are partitioned are described below. References are given for all those correlations available in technical literature, whereas new correlations obtained through the regression of published experimental data are presented in detail.

Water and salt component properties

The pure water properties, saturation pressure, density and internal energy are computed using the International Formulation Committee correlations (IFC, 1967) implemented in the TOUGH2 code. The formulation includes subregion 1 (subcooled water below $T = 350°C$), subregion 2 (superheated steam), and subregion 6 (saturation line up to $T = 350°C$). Dynamic viscosity of liquid water and steam is calculated, in the above subregions, using the correlation proposed by the International Association for the Properties of Steam (Meyer *et al.*, 1977), which reproduces the experimental data within

their uncertainty. The TOUGH2 code implements equations, given in the IFC formulation, which compute the viscosity within 2.5%.

We use the assumption that the NCG is only slightly soluble in the liquid phase so that brine density and viscosity are not influenced by the dissolved gas content. As far as the effect on the density of liquid phase is concerned, at 0°C the density of CO_2-saturated water with a CO_2 mass fraction as much as 0.07 is only 0.1% greater than that of pure water (Barton and Chou, 1993).

Brine vapour pressure. Haas (1976) presented a correlation to calculate the vapour pressure of sodium chloride solutions for salinities up to halite saturation in the temperature range from −11 to 300°C with a standard error of 0.32% of the observed pressure. The equations implemented in EWASG differ from the original ones used by Haas as the IFC correlation implemented in the TOUGH2 code has been used to compute the pure water saturation pressure. The lower limit of temperature ranges from 1°C for pure water up to 6°C for halite-saturated brine. Computed brine vapour pressure agrees with the tabulated data of Haas (1976). Figure 1 shows the computed brine vapour pressure vs temperature at different NaCl mass fractions up to 350°C. Figure 2 shows the results obtained above the validity range of the Haas equation compared to data published by Tanger and Pitzer (1989) at temperatures of 300, 325 and 350°C for salt mass fraction up to halite saturation: the data are reproduced within an error of 3%.

Brine density. Haas (1976) presented a correlation to calculate the density of vapour-saturated brine in the temperature range from 75 to 325°C, and salt mass fraction from 0 to 0.30, or up to halite saturation if the corresponding concentration is lower. The density is calculated with a stated precision of 2 kg/m^3 with respect to the experimental data. In EWASG the density of vapour-saturated pure water is computed using the IFC formulation: with this change the computed vapour-saturated brine density agrees with the tabulated data of Haas (1976). Figure 3 shows the computed vapour-saturated brine density from 5 to 350°C at various salt mass fractions compared with the data of Potter and

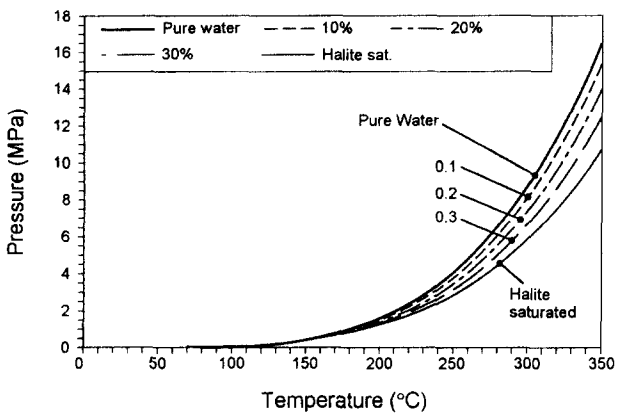

Fig. 1. Computed vapour pressure of NaCl solutions for salt mass fraction $X_L^{(2)}$ from 0 to halite saturation at 0–350°C.

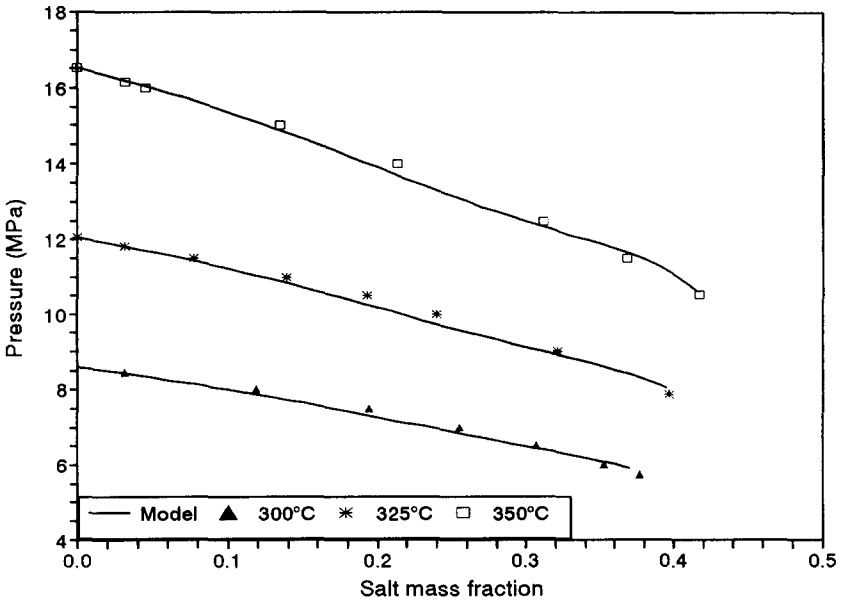

Fig. 2. Computed vapour pressure of NaCl solutions for salt mass fraction $X_L^{(2)}$ from 0 to halite saturation at 300, 325 and 350°C compared to the Tanger and Pitzer (1989) data.

Brown (1977). For the salinities considered in Fig. 3, the Potter and Brown data are reproduced with a maximum difference of 8.5 kg/m^3 in the temperature range of 25–300°C and salt mass fraction up to 0.25, and of 27 kg/m^3 up to 350°C and salt mass fraction up to 0.30.

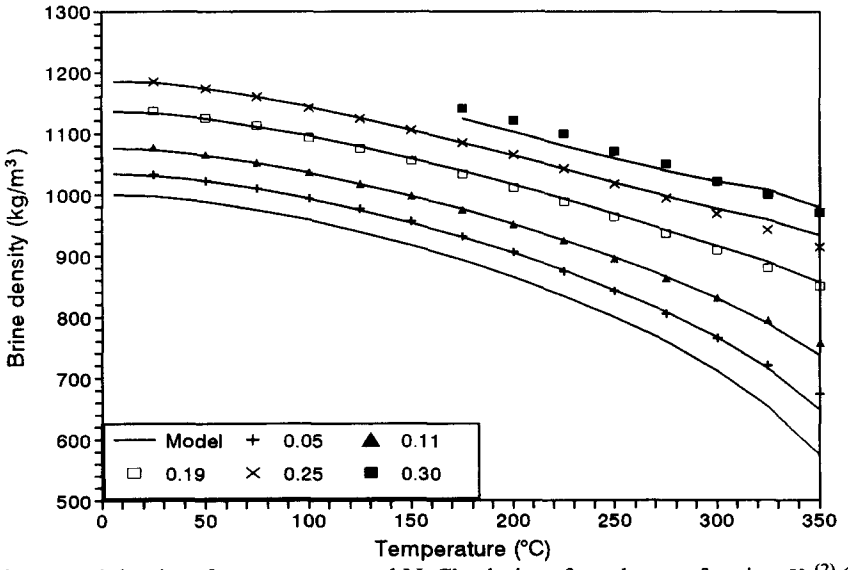

Fig. 3. Computed density of vapour-saturated NaCl solutions for salt mass fraction $X_L^{(2)}$ from 0 to 0.30 at 5–350°C compared with the Potter and Brown (1977) data.

The effect of pressure on brine density was estimated in the previous EWASG version (Battistelli *et al.*, 1993) with the assumption that brine compressibility is the same as that of pure water from the vapour-saturated pressure to current pressure. This assumption produces acceptable results at any salinity up to a temperature of about 250°C. As the critical temperature of pure water is approached, the water compressibility changes greatly, whereas this does not happen for brines having high salt content and thus a critical temperature much higher than that of water. Thus the correlation of brine compressibility published by Andersen *et al.* (1992) has been implemented to extend the temperature range to 350°C. Their correlation can be expressed as follows:

$$\rho_b(P, T, X_L^{(2)}) = \frac{\rho_{b\,sat}(P_{b\,sat}, T, X_L^{(2)})}{[1 + c_b(T, Y_L^{(2)})(P - P_{b\,sat})]} \tag{24}$$

where $Y_L^{(2)}$ is the mole fraction of sodium chloride in the liquid phase and c_b is the compressibility of sodium chloride solution

$$c_b(T, Y_L^{(2)}) = \frac{-1.6534 \times 10^{-10}}{(\theta^{1.25} - 5.6 Y_L^{(2)1.5} + 0.005)} \tag{25}$$

and θ is calculated using the critical temperature of the solution T_c

$$\theta = 1 - \frac{T + 273.15}{[T_c(X_L^{(2)}) + 273.15]} \tag{26}$$

The critical temperature of brine for a given salinity is calculated by an iterative procedure using an equation of salt mass fraction at critical conditions as a function of temperature given by a polynomial regression of the data presented by Sourirajan and Kennedy (1962). The critical temperature of pure NaCl of 1075°C has also been considered (McKibbin and McNabb, 1993)

$$X_c^{(2)} = \sum_{i=0}^{3} A(i) T_c^i \tag{27}$$

where the coefficients $A(i)$ have the following values:

$A(0) = -9.26825 \times 10^{-1}$
$A(1) = \ \ 4.30773 \times 10^{-3}$
$A(2) = -6.25612 \times 10^{-6}$
$A(3) = -3.64416 \times 10^{-9}$

The salt mass fraction data of Sourirajan and Kennedy are reproduced with a maximum error of 7.5×10^{-3}. The polynomial fit is shown in Fig. 4, where the data published by Tanger and Pitzer (1989) and Bischoff and Pitzer (1989) are also plotted for comparison.

Figure 5 shows the computed brine density for a salt mass fraction of 0.25 up to 350°C at the saturation pressure and at 20–80 MPa against the data of Potter and Brown (1977). Computed densities reproduce their smoothed experimental data in the temperature range of 0–300°C and up to a pressure of 60 MPa within an error of 1%, and up to 350°C and 80 MPa within an error of 5%.

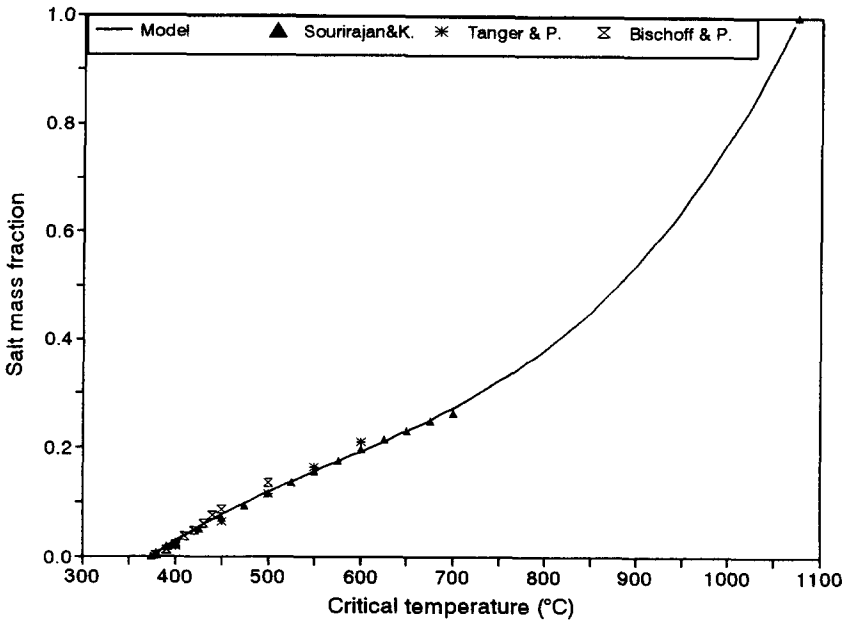

Fig. 4. Computed salt mass fraction as a function of critical temperature of NaCl solution compared with the Sourirajan and Kennedy (1962), Tanger and Pitzer (1989) and Bischoff and Pitzer (1989) data.

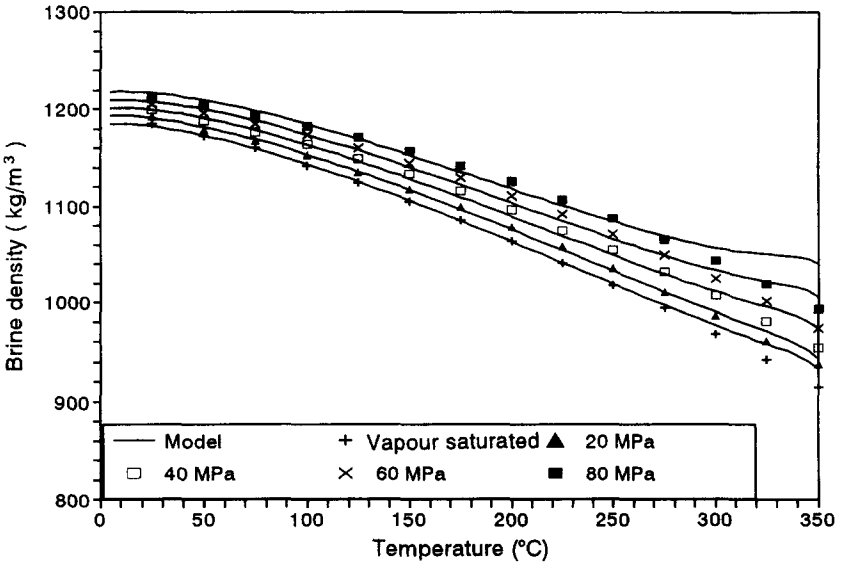

Fig. 5. Computed density of a 0.25 salt mass fraction NaCl solution at 5–350°C and from saturated conditions up to 80 MPa compared with the Potter and Brown (1977) data.

Brine enthalpy. The enthalpy of vapour-saturated sodium chloride solutions is calculated using the correlation of Michaelides (1981) based on the thermodynamic data presented by Silvester and Pitzer (1976) and Haas (1976). Michaelides states that its correlation reproduces the data with a resulting error not exceeding the discrepancies between the two sets of source data, evaluated in the order of 3%. The corrections of typing errors in the Michaelides paper, presented by Gudmundsson and Thrainsson (1989), have been considered. The compressed brine enthalpy is estimated assuming a similar pressure dependence for brine and pure water. The correlation should be applied in the temperature range 100–350°C. Below 100°C the error becomes large at high salinities.

Brine viscosity. Phillips *et al.* (1981) presented a correlation for the dynamic viscosity of brine for salt molality up to 5 over the temperature range 10–350°C and up to 50 MPa, reproducing the considered experimental data to an average of better than 2%. In EWASG the dynamic viscosity of pure water is computed using the International Association for the Properties of Steam (IAPS) interpolating equation (Meyer *et al.*, 1977). Computed dynamic viscosity agrees with the tabulated viscosity of vapour-saturated brine given by Phillips and coworkers as shown in Fig. 6.

Halite solubility. The concentration of solutions that are both vapour- and halite-saturated is evaluated using an equation by Potter quoted in Chou (1987), who recommends the use of this equation from 0 to 382°C. Figure 7 shows the computed concentration compared with the data published by Bischoff and Pitzer (1989).

Density and enthalpy of halite. Whereas the density of halite is only slightly dependent upon pressure, the effect of temperature is remarkable. The constant value of 2160 kg/m^3

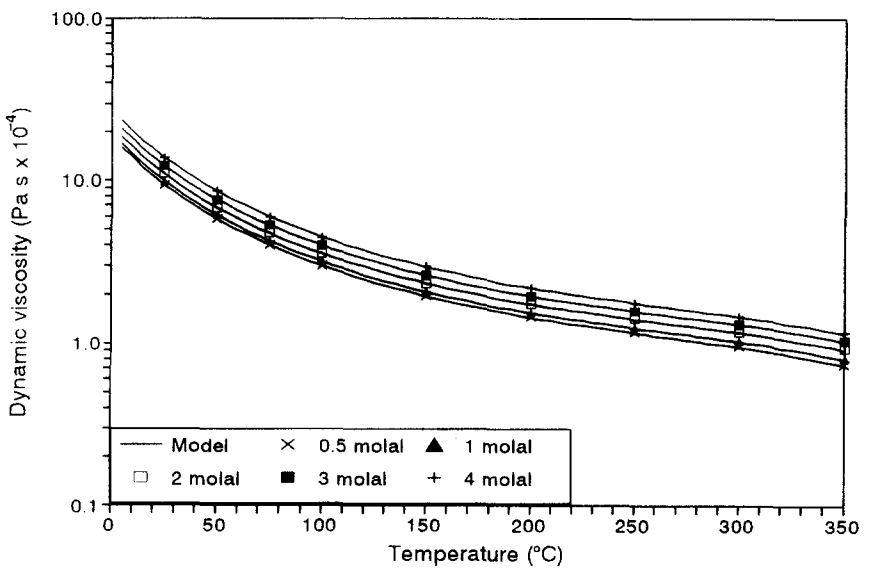

Fig. 6. Computed dynamic viscosity of vapour-saturated NaCl solutions from 0.5 to 4 molal at 5–350°C compared with the Phillips *et al.* (1981) data.

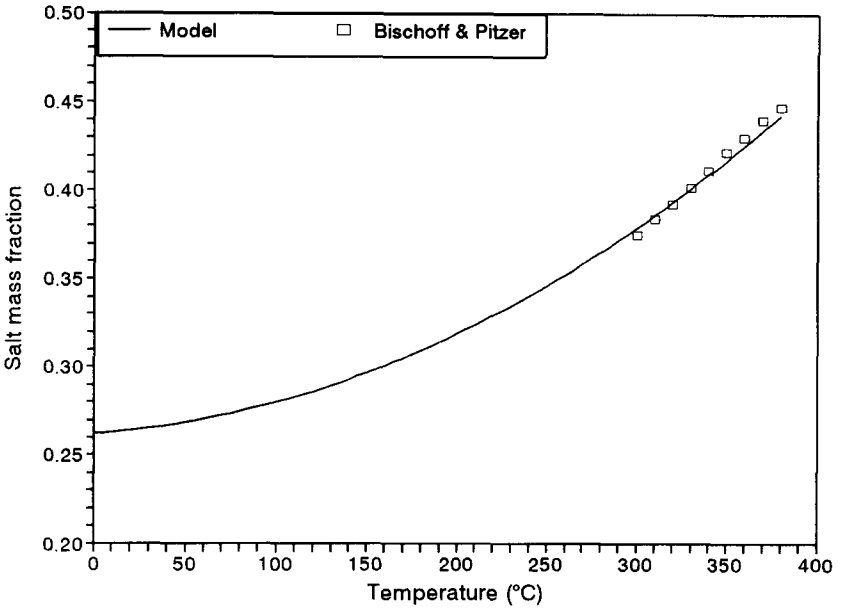

Fig. 7. Solubility of NaCl in water at 0–380°C compared with the Bischoff and Pitzer (1989) data.

used in the previous EWASG version has been substituted by the following equation accounting for the compressibility and expansivity of halite, where the reference density at 0°C and 0 Pa is 2165 kg/m^3:

$$\rho_S^{(2)}(P, T) = 2165 \exp(-1.2 \times 10^{-4} T + 4 \times 10^{-11} P) \tag{28}$$

The enthalpy of halite is calculated by integrating the equation of heat capacity at constant pressure reported by Silvester and Pitzer (1976). The equation is valid from 25 to 800°C (Palaban and Pitzer, 1987).

Carbon dioxide component

The equations used to calculate the carbon dioxide thermodynamic and transport properties are given below.

Density and enthalpy of gaseous carbon dioxide. The density and enthalpy of CO_2 as a function of temperature and its partial pressure are calculated from equations reported by Sutton and McNabb (1977). These equations are already used in the H_2O–CO_2 EOS module described by O'Sullivan *et al.* (1985) and implemented as EOS2 module in the TOUGH2 code. The computed density and enthalpy of gaseous CO_2 are plotted in Figs 8 and 9, respectively, as a function of CO_2 pressure at temperatures from 0 to 400°C against the values reported by the Encyclopedie des Gaz (1976). Computed densities reproduce the above values in the temperature range 0–400°C within an error of 1% up to a CO_2 pressure of 5 MPa, and in the range 200–400°C within an error of 6% up to a CO_2 pressure of 10 MPa. Computed enthalpies reproduce the tabulated values in the temperature range 0–400°C within an error of 10% up to a CO_2 pressure of 9 MPa, and in the range 200–400°C within an error of 5% up to a CO_2 pressure of 12 MPa.

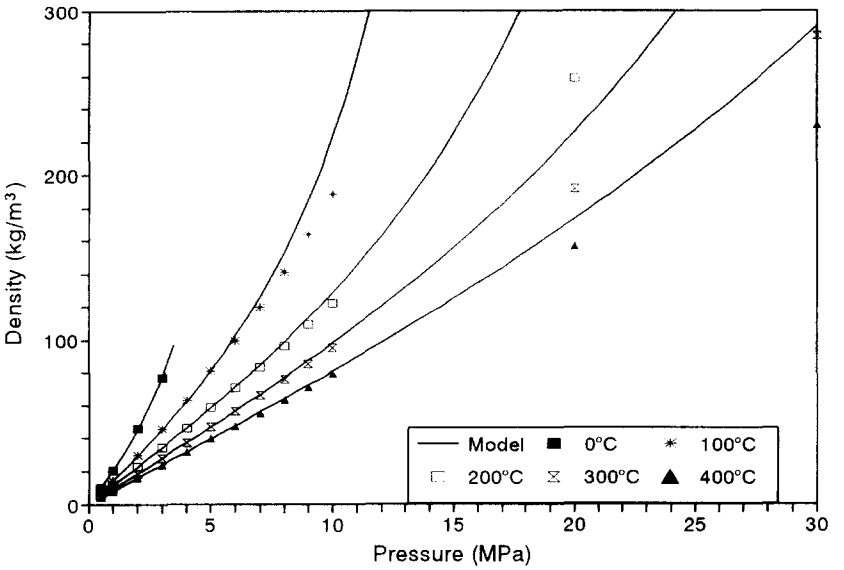

Fig. 8. Computed density of gaseous CO_2 at 0, 100, 200, 300 and 400°C up to 30 MPa compared with data reported by the Encyclopedie des Gaz (1976).

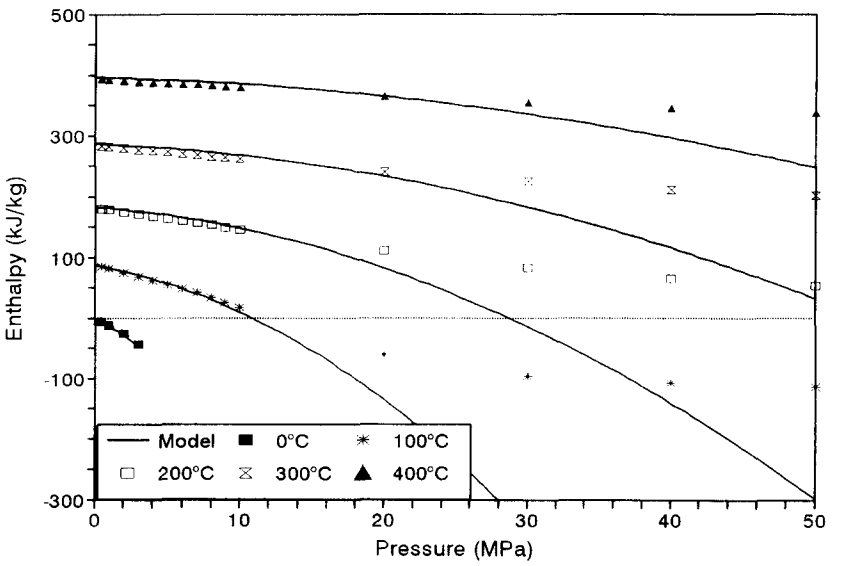

Fig. 9. Computed enthalpy of gaseous CO_2 at 0, 100, 200, 300 and 400°C up to 50 MPa compared with data reported by the Encyclopedie des Gaz (1976).

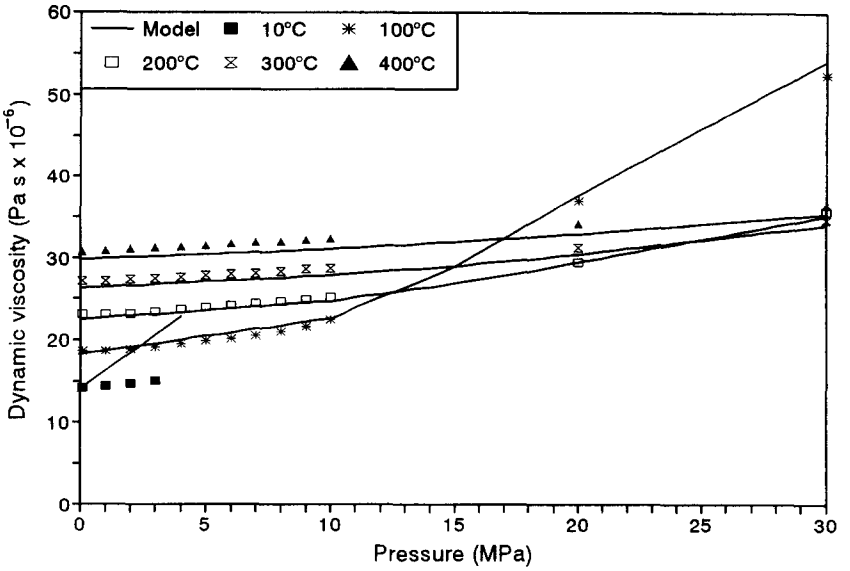

Fig. 10. Computed dynamic viscosity of gaseous CO_2 at 10, 100, 200, 300 and 400°C up to 30 MPa compared with data reported by the Encyclopedie des Gaz (1976).

Viscosity of gaseous carbon dioxide. The CO_2 dynamic viscosity is calculated using the correlation quoted by Pritchett *et al.* (1981) and already implemented in the TOUGH2 H_2O–CO_2 EOS module. Computed viscosity is plotted against the values reported by the Encyclopedie des Gaz (1976) as a function of CO_2 pressure for temperatures from 10 to 400°C in Fig. 10. Computed viscosities reproduce the tabulated values in the temperature range 100–400°C within an error of 4% up to a CO_2 pressure of 30 MPa. As the Pritchett *et al.* (1981) EOS module covers the temperature range 50–350°C, the viscosities computed with their correlation are affected by significant errors below 50°C.

Henry's law constant of carbon dioxide. Dissolution of carbon dioxide in pure water and sodium chloride brines is described using Henry's law and the concept of salting-out. Henry's constant is calculated as

$$K_{hb}(T, X_L^{(2)}) = K_h(T)10^{[m\, k_b(T)]} \tag{29}$$

where k_b is the salting-out coefficient and m is salt molality. Several approximations are implicit in this formulation: the most important is the application of the formula at other than very small solute gas concentrations. Henry's law constant for the dissolution of carbon dioxide in pure water and the salting-out coefficient are calculated using polynomial regressions of data from 0 to 300°C and for salinity up to 4.87 molal published by Cramer (1982). To extend the temperature range of Henry's constant correlation up to 350°C, the values recommended by D'Amore and Truesdell (1988) from 300°C to the critical point of water were also considered. The polynomial fit of Henry's constant is shown in Fig. 11 as a function of temperature for salt mass fractions of 0, 0.1, 0.2, 0.3 and at equilibrium with halite. The data by D'Amore and Truesdell (1988) are also plotted for comparison. The

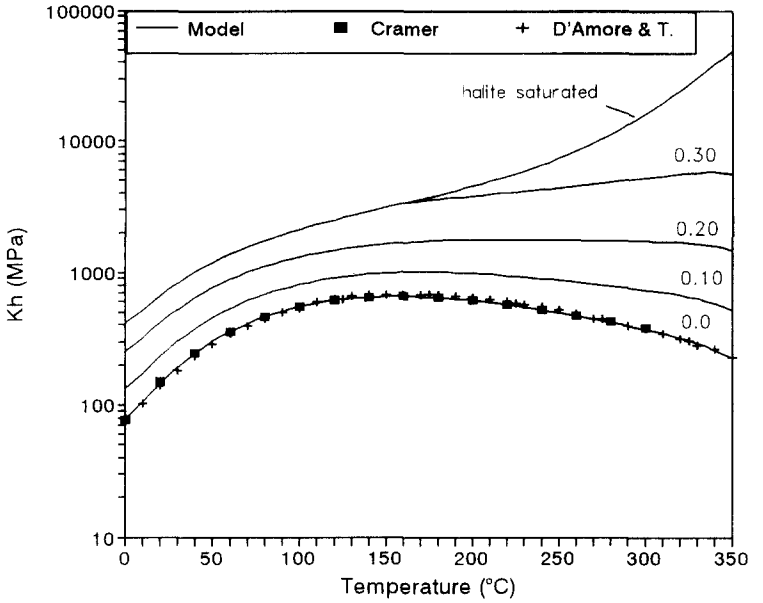

Fig. 11. Henry's law constant for CO_2 dissolved in NaCl solutions from 0 to halite saturation at 0–350°C. Computed Henry's law constant for pure water is compared with the Cramer (1982) and the D'Amore and Truesdell (1988) data.

maximum error for Henry's constant of pure water is 2.8% of data by Cramer. The equation is as follows:

$$K_h(T) = \sum_{i=0}^{5} B(i)T^i \tag{30}$$

where the coefficients $B(i)$ have the following values:

$B(0) = 7.83666 \times 10^7$
$B(1) = 1.96025 \times 10^6$
$B(2) = 8.20574 \times 10^4$
$B(3) = -7.40674 \times 10^2$
$B(4) = 2.18380$
$B(5) = -2.20999 \times 10^{-3}$

The equation for the salting-out coefficient is

$$k_b(T) = \sum_{i=0}^{4} C(i)T^i \tag{31}$$

The polynomial fit is shown in Fig. 12. Maximum error is 0.65%. The coefficients $C(i)$ have the following values:

$C(0) = 1.19784 \times 10^{-1}$
$C(1) = -7.17823 \times 10^{-4}$
$C(2) = 4.93854 \times 10^{-6}$
$C(3) = -1.03826 \times 10^{-8}$
$C(4) = 1.08233 \times 10^{-11}$

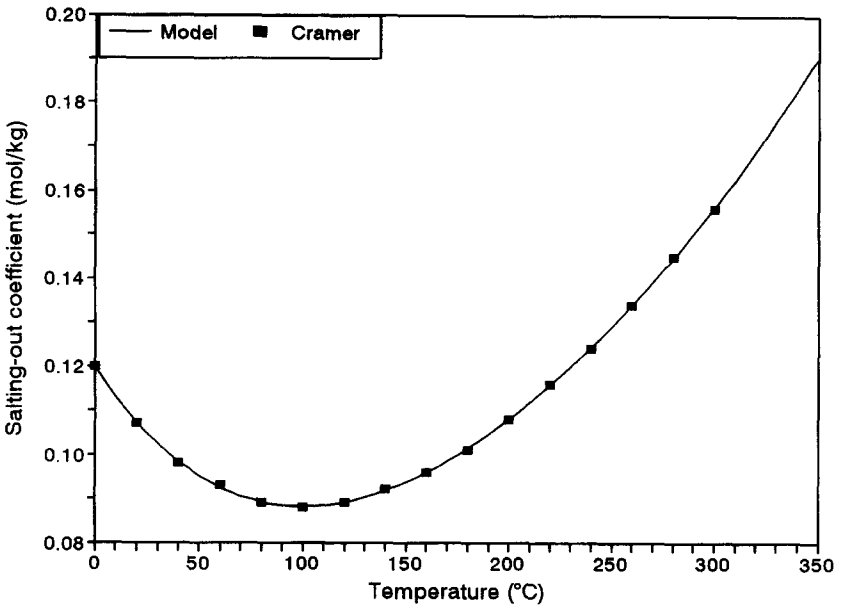

Fig. 12. Computed salting-out coefficient for CO_2 dissolved in NaCl solutions at 0–350°C compared with the Cramer (1982) data.

Enthalpy of dissolved carbon dioxide. The enthalpy of carbon dioxide dissolved in pure water is calculated adding the heat of solution to the enthalpy of carbon dioxide in the gaseous state, according to the expression

$$H_L^{(3)}(P^{(3)}, T) = H_G^{(3)}(P^{(3)}, T) + \Delta H_{sol}^{(3)}(T) \tag{32}$$

The heat of solution can be calculated using the expression of temperature dependence of the equilibrium constant for the chemical reaction of solution

$$CO_{2(G)} \rightarrow CO_{2(L)}$$

The equation that relates the heat of solution of a gas to its Henry's constant has been presented by, among others, Himmelblau (1959)

$$\left(\frac{\partial \ln K_h(T)}{\partial T}\right)_p = -\frac{\Delta H_{sol}^{(3)}(T)}{R(T + 273.15)^2 W^{(3)}} \tag{33}$$

In the above equation the molecular weight $W^{(3)}$ of CO_2 has been added to convert the heat of solution from J/mol to J/kg units. Equation (33) is used to derive the heat of solution for carbon dioxide in sodium chloride brines using Henry's constant K_{hb} given by equation (29). Figure 13 shows the heat of solution of CO_2 as a function of temperature at different salt mass fractions. The heat of solution data given by Ellis and Golding (1963) for pure water are also plotted for comparison.

Other optional NCG components

A brief description follows of the thermophysical properties of the other optional gases (i.e. air, CH_4, H_2 and N_2) now implemented in EWASG.

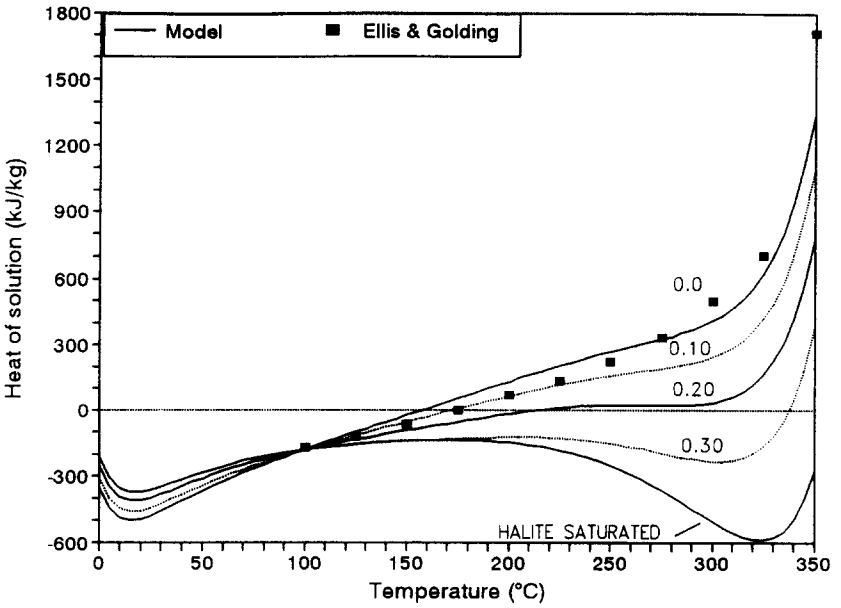

Fig. 13. Heat of solutions for CO_2 dissolved in NaCl solutions from 0 to halite saturation at 0–350°C compared with the Ellis and Golding (1963) data for pure water.

The density of the above gases is calculated using the perfect gas law. The assumption of perfect gas behaviour is also used to calculate specific enthalpy in the gaseous phase as a function of temperature according to the equations presented by Irvine and Liley (1984).

The dynamic viscosity of gaseous CH_4 and N_2 is also given as a function of temperature using the equations of Irvine and Liley (1984). Viscosity of H_2 is computed using the same subroutine implemented in the EOS5 module of the standard TOUGH2 code; the viscosity of air–vapour mixtures is also calculated using the same subroutine of the EOS3–EOS4 modules (Pruess, 1991a).

Henry's law constant is given as a function of temperature using polynomial regressions of data published by D'Amore and Truesdell (1988) for N_2 and H_2, and by Cramer (1982) for O_2 and CH_4. The salting-out effect is calculated using polynomial regressions of data published by Cramer (1982) for O_2 and CH_4 and by Cygan (1991) for N_2. The effects of salinity on H_2 solubility have been neglected. The heat of solution for all four gases is computed using equation (33) by derivation of the appropriate Henry's law constant.

Our main problem now being to enhance the geothermal version of the code, we have not tried to implement more accurate correlations for these gases. The P–T range of applicability of the thermophysical formulation is also limited by the fact that the formulation is based on the perfect gas law.

VAPOUR PRESSURE LOWERING

The vapour pressure of water in a porous medium at a given temperature tends to be smaller than above a flat surface of bulk water. This so-called vapor pressure lowering is caused by capillary and vapour adsorption effects, collectively referred to here as suction pressure effects (Pruess and O'Sullivan, 1992). VPL phenomena are believed to be of great

importance in determining the in-place and extractable fluid reserves of vapour-dominated geothermal reservoirs.

VPL due to suction pressure has been included in the EWASG module, as expressed by Kelvin's equation, in a way similar to that used by Pruess (1991a) for the EOS4 module for air–water mixtures of the TOUGH2 code. Salinity effects have been considered by following the simplified derivation of Kelvin's equation presented by Calhoun *et al.* (1949). The possible effects of NCG have been neglected in the present formulation, as in the EOS4 module (Pruess, 1991a). The combined effect of suction pressure and salinity is then described by considering the liquid-phase thermodynamic properties, as affected by salt content, in Kelvin's equation

$$P^{(1)}(T, S_{La}, X_L^{(2)}) = f_{VPL}(T, S_{La}, X_L^{(2)}) P_{b\,sat}(T, X_L^{(2)}) \tag{34}$$

where f_{VPL}, the VPL factor, is given by

$$f_{VPL} = \exp\left[\frac{W^{(1)} P_{cap}(S_{La})}{\rho_L(P_L, T, X_L^{(2)}) R(T + 273.15)}\right] \tag{35}$$

The capillary pressure is evaluated considering the "active saturation" of liquid phase S_{La}. Active saturations of flowing phases are defined as follows:

$$S_{\beta a} = S_\beta / (1 - S_S) \tag{36}$$

where β = L,G and

$$S_{La} + S_{Ga} = 1 \tag{37}$$

As solid deposition occurs on the surface of rock grains and fractures, the narrow pore spaces will be affected first, followed by the wider ones as solid saturation increases. As the capillary pressure is a function of the pore structure and size distribution, in addition to the changes in the properties of fluid phases present, we can also expect that, as a result of solid deposition, the shape of the capillary pressure function will change as a function of solid phase saturation. The above approach represents only a first attempt to account for solid-phase appearance effect among the models that could be considered.

In the presence of VPL effects due to suction pressure, the liquid phase can be present under conditions where vapour partial pressure plus the gas phase total pressure are less than the brine saturation pressure. This is shown in Fig. 14, where the vapour pressure of pure water for different liquid-phase saturations is plotted versus temperature. The VPL factor in Fig. 14 was calculated with equation (34) using the capillary pressure function given by Pruess and O'Sullivan (1992), which is intended to be representative of tight rock formations present in vapour-dominated reservoirs. The capillary pressure relationship was experimentally obtained by Peters *et al.* (1984) on a sample of tight welded tuff collected at Yucca Mountain, Nevada. In fact, most of the data presented by Peters *et al.* were obtained by vapour pressure measurements, which they then inverted by means of Kelvin's equation [equation (35)] to obtain equivalent capillary pressures. Figure 14 clearly shows that due to VPL effects two-phase conditions can exist at pressure well below the saturation pressure.

The density, viscosity and enthalpy of brine in a liquid–gas mixture with VPL effects are thus calculated considering the liquid-phase pressure given by (Pruess, 1991a)

$$P_L = \max(P_G, P_{b\,sat}) \tag{38}$$

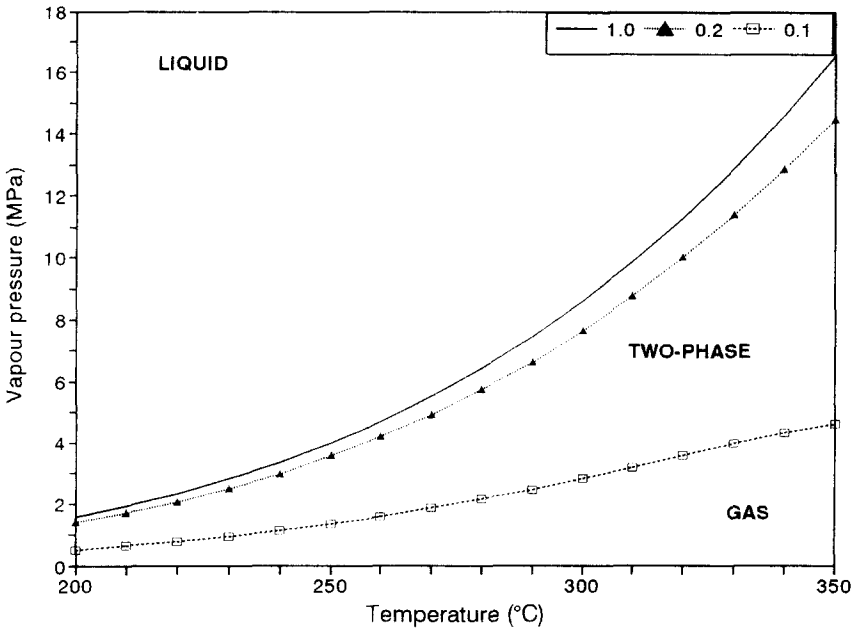

Fig. 14. Vapour pressure of pure water at 200–350°C as a function of liquid phase saturation S_L with VPL effects due to suction pressure. The vapour pressure is computed by the capillary pressure function used by Pruess and O'Sullivan (1992).

The liquid-phase pressure determined with the above condition is also used to calculate the brine density for Kelvin's equation.

The inclusion of VPL also affects the tests for the appearance of phases and the calculation of thermophysical properties of steam. Equations (11), (16), (20) and (22) are modified accordingly by multiplying the vapour brine pressure by the VPL factor f_{VPL}. VPL capabilities can be invoked simply by setting *on* a switch from the input deck.

MODELLING OF PERMEABILITY REDUCTION

Changes in formation permeability due to precipitation or dissolution of halite are modelled using the porosity–permeability correlations given in the paper by Verma and Pruess (1988). They considered idealized models of permeable media to correlate the relative changes in permeability to the relative changes in porosity caused by the redistribution of a mineral in the pore space. The medium is assumed to have a set of non-intersecting flow channels with either circular, tubular, or planar cross-sections as shown in Fig. 15.

As cross-sections of actual flow channels are highly variable, minor changes in average porosity could be expected to cause drastic permeability changes, as a result of the closure of the narrow portions of pore throats. The "series models" shown in Fig. 15c and d are able to represent, albeit in a rough way, the presence of "bottle-necks" in the flow channels. Because of this feature the permeability of a porous medium can reduce to zero at a finite porosity, indicated as "critical porosity".

The EWASG module implements all the permeability–porosity relationships

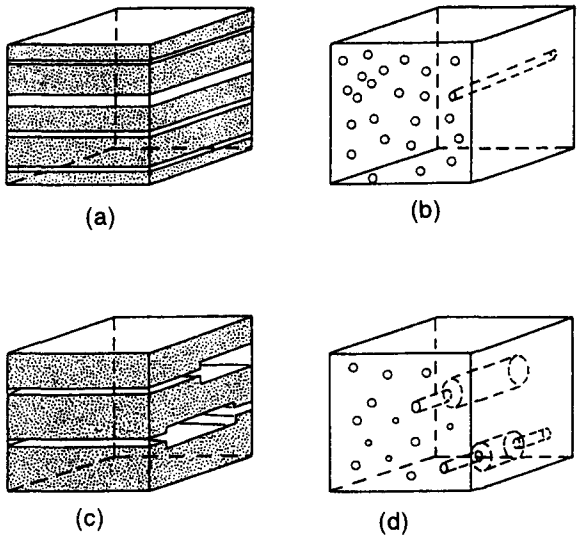

Fig. 15. Idealized models of permeable media. (a) and (b) represent the straight capillaric models, and (c) and (d) the series models (after Verma and Pruess, 1988).

corresponding to the pore models shown in Fig. 15. Other models based on statistical distributions of pore dimensions are described by Verma and Pruess (1988).

The precipitation/dissolution of the solid salt phase changes the original permeability distribution in the simulation domain. Thus problems may arise with regard to the proper averaging scheme of reduced permeability at the interface of two adjacent grid blocks even for an initially homogeneous porous medium.

The discretized version of the mass flux term for the generic component (κ) in the flowing phase β takes the following form (Pruess, 1991a):

$$F_{\beta,nm} = -k_{nm}\left(\frac{k_{r\beta}\rho_\beta}{\mu_\beta}\right)_{nm}\left(\frac{P_{\beta,n} - P_{\beta,m}}{d_{nm}} - \rho_{\beta,nm}g_{nm}\right) \tag{39}$$

where the subscripts nm denote a suitable averaging at the interface of adjacent grid blocks. The available averaging schemes in the standard TOUGH2 code for phase mobility $(k_{r\beta}/\mu_\beta)_{nm}$ are the upstream weighting and arithmetic averaging, whereas upstream and harmonic averaging are available for rock permeability k_{nm}.

The initial implementation of permeability reduction in EWASG (Battistelli *et al.*, 1993) followed that used by Verma and Pruess (1988) for water–silica mixtures. The permeability reduction was applied to the relative permeabilities of liquid and gas phases. Consequently, the mobility–permeability reduction factor product was averaged at the grid blocks' interface using the averaging schemes available for the mobility term. This choice derived from the fact that no changes to TOUGH2 subroutines other than that contained in the EOS module were required.

A more rigorous approach is followed in the present EWASG version. The permeability reduction has been applied to the rock permeability, so that the permeability–permeability reduction factor product can be averaged at the grid block interface with the averaging schemes already available for absolute rock permeability. This modification required

changes to the MULTI subroutine that assembles the balance equations. The revised MULTI subroutine is now part of the EWASG module.

The reduction of rock permeability also affects the withdrawal of fluid from sinks simulated using the wellbore on deliverability option available in the TOUGH2 code. The mass rate flowing toward a wellbore is computed according to Pruess (1987)

$$q = \sum_{\beta=\mathrm{L,G}} \frac{k_{\mathrm{r}\beta}}{\mu_\beta} \rho_\beta PI(P_\beta - P_{\mathrm{wb}}) \tag{40}$$

Under the assumption of steady, horizontal, single-liquid flow in an homogeneous medium, for which Darcy's law is applicable, the PI can be evaluated as

$$PI = \frac{2\pi kh}{\ln(r_{\mathrm{e}}/r_{\mathrm{w}}) + s} \tag{41}$$

where r_{e} is the distance at which the pressure P_β is acting. Several approaches are available to determine the wellblock radius r_{e}. Reference is made to the work by Hadgu *et al.* (1995), who examined the problem specifically for implementation in the TOUGH2 code. They also discussed the use of equation (40) for two-phase flow. It needs to be modified for cases in which the pressure difference between the wellblock and the wellbore is such that the evaluation of thermophysical parameters at wellblock conditions does not give an accurate calculation of extracted rate and enthalpy.

Equation (41) shows that PI is directly proportional to wellblock permeability and thus it is affected by permeability changes resulting from precipitation/dissolution of solid salt. In calculating the rate withdrawal with the wellbore on deliverability option, a normalized PI is used, obtained by multiplying the PI by the permeability reduction factor. This modification required changes to the QU subroutine that computes the contributions arising from sinks and sources. The revised QU subroutine is now part of the EWASG module.

CONCLUSIONS

An equation-of-state package for ternary mixtures of H_2O, NaCl, and a single slightly soluble NCG has been developed for the simulation of the thermophysical behaviour of saline systems. The package, called EWASG, has been incorporated into the general-purpose multiphase fluid and heat flow code TOUGH2, belonging to the MULKOM family of computer codes developed at Lawrence Berkeley National Laboratory. Only minor changes to subroutines MULTI and QU were needed. The modified versions of these subroutines have been added to the EWASG module.

Although only the thermophysical properties of CO_2 have been described, the NCG being of major interest for geothermal applications, in the EWASG module the NCG can be chosen as air, CO_2, CH_4, H_2, or N_2. Possible applications of the module include the simulation of systems such as geothermal reservoirs, the saturated/unsaturated zone, natural gas reservoirs, aquifer gas storage reservoirs, and nuclear waste repositories where the flow of saline brine occurs.

The EWASG formulation includes a comprehensive suite of multiphase mixture effects, including density, viscosity, enthalpy and vapour pressure lowering due to salinity effects, reduction in NCG solubility and related heat of solution due to salinity, and porosity and permeability changes from the precipitation/dissolution of halite. The effects of dissolved

salts on the vapour pressure lowering due to suction pressure effects, as described by Kelvin's equation, are also considered, whereas those of NCG are neglected.

The modelling approach followed in developing the EWASG module has been discussed, together with the correlations employed to calculate the thermophysical properties of multiphase H_2O–NaCl–CO_2 mixtures, which can be used to simulate the thermodynamic behaviour of commonly exploited geothermal reservoirs.

The range of applicability of the thermophysical formulation is: temperatures from 100 to 350°C, total pressure up to 80 MPa, partial pressure of CO_2 up to 10 MPa, and salt mass fraction up to halite saturation. The lower temperature limit (100°C) is only a result of the correlation used for brine enthalpy, otherwise it could be less than 10°C. The accuracy obtainable in computing any thermophysical property of components in the mixture has been indicated. Some of the correlations presented are actually employed outside the original range of conditions for which they have been formulated. Whenever possible, the accuracy has also been evaluated outside the original range of conditions.

It is not easy to assess the global accuracy of a module for a three-component mixture as a function of temperature, pressure, and composition. For example, the correlations used to calculate the properties of gaseous CO_2 have an accuracy that decreases at decreasing temperature and increasing pressure: CO_2 viscosity at 10°C and 4 MPa is computed with an error of about 43%. It is also true that these conditions, low temperature and high CO_2 pressure, are not likely to occur in a natural system: at the same temperature but at a partial pressure of only 1 MPa the error decreases to about 14%.

Efforts should be directed towards improving accuracy in the calculation of brine properties at a salt mass fraction exceeding 0.25 and in the implementation of a new correlation for brine enthalpy, valid below 100°C. The subroutine-by-subroutine structure employed to evaluate the thermophysical properties of mixture phases allows easy updating of the module once more reliable experimental data and correlations are available.

Acknowledgements—This work was supported by Aquater SpA of the ENI Group, by the International Institute for Geothermal Research of the Italian National Research Council (CNR), and by the Assistant Secretary for Conservation and Renewable Energy, Geothermal Division, of the U.S. Department of Energy under contract No. DE-AC03-76SF00098.

REFERENCES

Alkan, H., Babadagli, T. and Satman, A. (1995) The prediction of the PVT/phase behavior of the geothermal fluid mixtures. *Proceedings World Geothermal Congress* 1995, Florence, volume 3, pp. 1659–1665.

Andersen, G., Probst, A., Murray, L. and Butler, S. (1992) An accurate PVT model for geothermal fluids as represented by H_2O–NaCl–CO_2 mixtures. *Proceedings 17th Workshop on Geothermal Reservoir Engineering*, Stanford, CA, pp. 239–248.

Barton, P. B. and Chou, I.-M. (1993) Calculation of the vapor-saturated liquidus for the NaCl–CO_2–H_2O system. *Geochimica et Cosmochimica Acta* **57**, 2715–2723.

Battistelli, A. (1991) PROFILI code: the thermodynamic package for H_2O–NaCl–CO_2 fluid mixtures. Aquater Report H 6046, San Lorenzo in Campo, Pesaro, Italy, 32 pp.

Battistelli, A., Calore, C. and Pruess, K. (1993) A fluid property module for the TOUGH2 simulator for saline brines with non-condensible gas. *Proceedings 18th Workshop on Geothermal Reservoir Engineering*, Stanford, CA, pp. 249–259.

Battistelli, A., Calore, C. and Pruess, K. (1995) Vapor pressure lowering effects due to salinity and suction pressure in the depletion of vapor-dominated geothermal reservoirs.

Proceedings TOUGH '95 Workshop, Lawrence Berkeley Laboratory Report LBL-37200, Berkeley, CA, pp. 77–83.

Bischoff, J. L. and Pitzer, K. S. (1989) Liquid–vapor relations for the system NaCl–H_2O: summary of the surface P–T–x from 300° to 500°C. *American Journal of Science* **289**, 217–248.

Calhoun, J. C., Lewis, M. and Newman, R. C. (1949) Experiments on the capillary properties of porous solids. *Transactions AIME* **186**, 189–196.

Calore, C., Battistelli, A. and Pruess, K. Analysis of salt effects on the depletion of fractured reservoirs by means of the simulator TOUGH2/EWASG. *Geothermics* (in preparation).

Chou, I. M. (1987) Phase relations in the system NaCl–KCl–H_2O. III: solubilities of halite in vapor-saturated liquids above 445°C and redetermination of phase equilibrium properties in the system NaCl–H_2O. *Geochimica et Cosmochimica Acta* **51**, 1965–1975.

Cramer, S. D. (1982) The solubility of methane, carbon dioxide and oxygen in brines from 0° to 300°C. US Bureau of Mines, Report No. 8706, U.S.A., 16 pp.

Cygan, R. T. (1991) The solubility of gases in NaCl brine and a critical evaluation of available data. Sandia Report SAND90-2848.UC-721, Sandia National Laboratory, Albuquerque, NM, 99 pp.

D'Amore, F. and Truesdell, A. H. (1988) A review of solubilities and equilibrium constants for gaseous species of geothermal interest. *Science Geological Bulletin* **41**(3–4), 309–332.

Ellis, A. J. and Golding, R. M. (1963) The solubility of carbon dioxide above 100°C in water and in sodium chloride solutions. *American Journal of Science* **261**, 47–60.

Encyclopedie des Gaz (1976) *Dioxide de Carbon*, pp. 333–368. Elsevier, Amsterdam.

Gudmundsson, J.-S. and Thrainsson, H. (1989) Power potential of two-phase geothermal wells. *Geothermics* **18**, 357–366.

Haas Jr, J. L. (1976) Physical properties of the coexisting phases and thermochemical properties of the H_2O component in boiling NaCl solutions. USGS Bulletin 1421-A, Washington, D.C., 73 pp.

Hadgu, T., Zimmerman, R. W. and Bodvarsson, G. S. (1995) Coupled reservoir–wellbore simulation of geothermal reservoir behaviour. *Geothermics* **24**, 145–166.

Himmelblau, D. M. (1959) Partial molal heats and entropies of solution for gases dissolved in water from the freezing to the near critical point. *Journal of Physical Chemistry* **63**, 1803–1808.

International Formulation Committee (1967) A formulation of the thermodynamic properties of ordinary water substance. IFC Secretariat, Dusseldorf.

Irvine Jr, T. F. and Liley, P. E. (1984) *Steam and Gas Tables with Computer Equations*. Academic Press, Orlando, FL, 185 pp.

Kissling, W. M., White, S. P., O'Sullivan, M. J., Bullivant, D. P. and Brown, K. L. (1996) Modelling chloride and CO_2 chemistry at the Wairakei geothermal field, New Zealand. *Proceedings 21st Workshop on Geothermal Reservoir Engineering*, Stanford, CA, pp. 217–223.

McKibbin, R. and McNabb, A. (1993) Modelling the phase boundaries and fluid properties of the system H_2O–NaCl at high temperatures and pressures. *Proceedings 15th New Zealand Geothermal Workshop*, Auckland, pp. 267–273.

McKibbin, R. and McNabb, A. (1995) Mathematical modelling of non-condensible gases in hot dense brines: the system H_2O–NaCl–CO_2. *Proceedings 17th New Zealand Geothermal Workshop*, Auckland, pp. 255–262.

Meyer, C. A., McClintock, R. B., Silvestri, G. J. and Spencer, R. C. (1977) *ASME Steam Tables*. The American Society of Mechanical Engineers, New York, 329 pp.

Michaelides, E. E. (1981) Thermodynamic properties of geothermal fluids. *Geothermal Resources Council Transactions* **5**, 361–364.

Moya, S. L., Ruiz, J. N., Aragon, A. and Iglęsias, E. R. (1995) Finite differences numerical model for mass and energy transport in geothermal reservoirs with carbon dioxide. *Geotermia, Revista Mexicana de Geoenergia* **11**(1), 37–51.

O'Sullivan, M. J., Bodvarsson, G. S., Pruess, K. and Blakeley, M. R. (1985) Fluid and heat flow in gas-rich geothermal reservoirs. *Society of Petroleum Engineers Journal* **25**, 215–226.

Palaban, R. T. and Pitzer, K. S. (1987) Thermodynamics of concentrated electrolyte mixtures and the prediction of mineral solubilities to high temperatures for mixtures in the system Na–K–Mg–Cl–SO_4–OH–H_2O. *Geochimica et Cosmochimica Acta* **51**, 2429–2443.

Peters, R. R., Klavetter, E. A., Hall, I. J., Blair, S. C., Heller, P. R. and Gee, G. W. (1984) Fracture and matrix hydrologic characteristics of tuffaceous materials from Yucca Mountain, Nye County, Nevada. Sandia Report SAND84-1471, Sandia National Laboratories, Albuquerque, NM.

Phillips, S. L., Igbene, A., Fair, J. A., Ozbek, H. and Tavana, M. (1981) A technical databook for geothermal energy utilization. Lawrence Berkeley Laboratory Report LBL-12810, Berkeley, CA, 46 pp.

Potter, R. W. and Brown, D. L. (1977) The volumetric properties of aqueous sodium chloride solutions from 0° to 500°C at pressures up to 2000 bars based on a regression of available data in the literature. USGS Bulletin 1421-C, Washington, D.C., 36 pp.

Pritchett, J. W. (1993) STAR User's manual. Appendix F.1—The "BRNGAS" equation-of-state. S-Cubed Report SSS-TR-89-10242, revision A, La Jolla, CA, 26 pp.

Pritchett, J. W., Rice, M. H. and Riney, T. D. (1981) Equation-of-state for water–carbon dioxide mixtures: implications for Baca reservoir. Report DOE/ET/27163-8, UC-66a, La Jolla, CA, 53 pp.

Pruess, K. (1983) Development of the general purpose simulator MULKOM. In Annual Report 1982, Earth Sciences Div., Lawrence Berkeley Laboratory Report LBL-15500, Berkeley, CA, pp. 133–134.

Pruess, K. (1987) TOUGH User's guide. Nuclear Regulatory Commission, Report NUREG/CR-4645 (also Lawrence Berkeley Laboratory Report LBL-20700, Berkeley, CA), 78 pp.

Pruess, K. (1991a) TOUGH2—a general-purpose numerical simulator for multi-phase fluid and heat flow. Lawrence Berkeley Laboratory Report LBL-29400, Berkeley, CA, 102 pp.

Pruess, K. (1991b) EOS7—an equation-of-state module for the TOUGH2 simulator for two-phase flow of saline water and air. Lawrence Berkeley Laboratory Report LBL-31114, Berkeley, CA, 17 pp.

Pruess, K. (ed.), (1995) Proceedings of the TOUGH Workshop '95. Lawrence Berkeley Laboratory Report LBL 37200, Berkeley, CA, 365 pp.

Pruess, K. and O'Sullivan, M. (1992) Effects of capillarity and vapor adsorption in the depletion of vapor-dominated geothermal reservoirs. *Proceedings 17th Workshop on Geothermal Reservoir Engineering*, Stanford, CA, pp. 165–174.

Satik, C., Walters, M. and Horne, R. N. (1996) Adsorption characteristics of rocks from vapor-dominated geothermal reservoir at The Geysers, CA. *Proceedings 21st Workshop on Geothermal Reservoir Engineering*, Stanford, CA, pp. 469–479.

Shook, G. M. (1995) Development of a vapor-dominated reservoir with a "high-temperature" component. *Geothermics* **24**, 489–506.

Silvester, L. F. and Pitzer, K. S. (1976) Thermodynamics of geothermal brines—I.

Thermodynamic properties of vapor-saturated NaCl (aq) solutions from 0–300°C. Lawrence Berkeley Laboratory Report LBL-4456, Berkeley, CA, 62 pp.

Sourirajan, S. and Kennedy, G. C. (1962) The system H_2O–NaCl at elevated temperatures and pressures. *American Journal of Science* **260**, 115–141.

Sutton, F. M. and McNabb, A. (1977) Boiling curves at Broadlands field. *New Zealand Journal of Science* **20**, 333–337.

Tanger, J. C. and Pitzer, K. S. (1989) Thermodynamics of NaCl–H_2O: a new equation of state for the near-critical region and comparisons with other equations for adjoining regions. *Geochimica et Cosmochimica Acta* **53**, 973–987.

Verma, A. and Pruess, K. (1988) Thermohydrological conditions and silica redistribution near high-level nuclear wastes emplaced in saturated geological formations. *Journal of Geophysical Research* **93**(B2), 1159–1173.

White, S. P. (1994) Transport of reacting chemicals in a two-phase reservoir. *Proceedings 16th New Zealand Geothermal Workshop*, Auckland, pp. 175–180.

White, S. P. (1995) Multiphase non-isothermal transport of systems of reacting chemicals. *Water Resources Research* **32**(7), 1761–1772.

Zyvoloski, G. A. and O'Sullivan, M. J. (1980) Simulation of a gas-dominated, two-phase geothermal reservoir. *Society of Petroleum Engineers Journal* **20**, 52–58.